MITSUBISHI ELECTRIC RESEARCH LABORATORIES
https://www.merl.com

Power Optimizing Control of Multi-Zone Heat Pumps

Bortoff, Scott A.; Burns, Daniel J.; Laughman, Christopher R.; Qiao, Hongtao; Danielson, Claus; Goldsmith, Abraham; Di Cairano, Stefano

TR2018-127 August 25, 2018

Abstract

We derive a power-optimizing output feedback controller for a multi-zone heat pump that (1) regulates individual zone temperatures, rejecting unknown heat load disturbances, (2) regulates condenser subcooling and (3) the compressor discharge temperature, and (4) minimizes electrical power consumption at steady-state operating conditions. The design is a cascade of a linear inner-loop and a nonlinear outer-loop. The inner-loop is designed for robust disturbance rejection using H-infinity loop-shaping methods. The outer-loop uses a model of compressor and fan power consumption and a gradient descent feedback to drive the system to its powerminimizing equilibrium for constant values of references and disturbances. The controller uses only temperature measurements for feedback; refrigerant pressure sensors, which are not present in many products for cost reasons, are not required. A proof of exponential stability is provided and preliminary experimental tests demonstrate satisfactory transient responses for a commercial multi-zone heat pump.

IEEE Conference on Control Technology and Applications

Power Optimizing Control of Multi-Zone Heat Pumps

Scott A. Bortoff, Daniel J. Burns, Christopher R. Laughman, Hongtao Qiao, Claus Danielson, Abraham Goldsmith, and Stefano Di Cairano [1]

***Abstract*— We derive a power-optimizing output feedback controller for a multi-zone heat pump that (1) regulates individual zone temperatures, rejecting unknown heat load disturbances, (2) regulates condenser subcooling and (3) the compressor discharge temperature, and (4) minimizes electrical power consumption at steady-state operating conditions. The design is a cascade of a linear inner-loop and a nonlinear outer-loop. The inner-loop is designed for robust disturbance rejection using H_∞ loop-shaping methods. The outer-loop uses a model of compressor and fan power consumption and a gradient descent feedback to drive the system to its power-minimizing equilibrium for constant values of references and disturbances. The controller uses only temperature measurements for feedback; refrigerant pressure sensors, which are not present in many products for cost reasons, are not required. A proof of exponential stability is provided and preliminary experimental tests demonstrate satisfactory transient responses for a commercial multi-zone heat pump.**

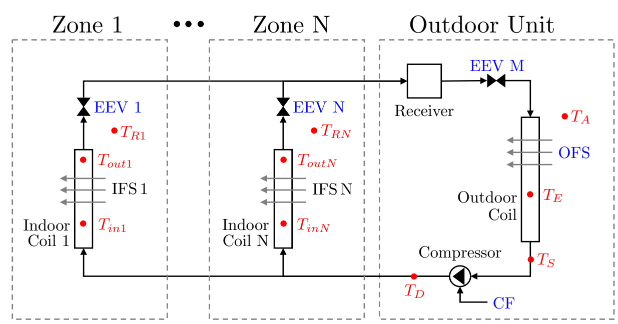

Fig. 1. VCS system showing the location of the temperature sensors (red) and control variables (blue). Airflow across each coil, indicated with grey arrows, is modulated by variable speed fans (not shown). In heating mode, refrigerant flow is clockwise.

I. INTRODUCTION

Building HVAC systems account for approximately 15% of global energy consumption, resulting in about 10% of global greenhouse emissions [1], and represent a big target for energy efficiency improvement. With the growth in renewable electricity generation, electric heat pumps in particular will play an increasingly important role in supplanting fossil fuel-based boilers and furnaces. Proper control is critical for these systems to meet their potential, especially as they become larger in scale and broader in application.

The conventional approach to heat pump control is to use a combination of single-variable feedback loops and schedules for key process variables (e.g., evaporator pressure [2]) to minimize energy consumption. These methods are effective for single-zone heat pumps which have perhaps 3-4 control variables. But multi-zone systems, some with dozens of zones, are large-scale, multivariable, interactive and possess considerable model uncertainty, putting them beyond the capability of conventional control laws. Distributed control has been proposed as a potential solution [3], as has model predictive control (MPC) because it considers multivariable systems with constraints and it explicitly optimizes a cost function [4]. But MPC requires a real-time solution to an optimization problem that may curb its application, although recent results for fast and efficient optimization are promising [5]. Furthermore, MPC for vapor compression systems (VCS) may provide poor robustness margins [6] if it is based on an LQR-type cost function and state estimates are used for feedback.

[1] Authors are with Mitsubishi Electric Research Laboratories, Cambridge, MA, USA {bortoff, burns, laughman, qiao, danielson, goldsmith, dicairano}@merl.com

In this paper, we present a multivariable control architecture for a multi-zone air-to-air heat pump which achieves independent zone temperature control, regulates key internal process variables, minimizes the system power consumption, and uses only temperature sensors for feedback. The architecture is a cascade consisting of an inner-loop designed via H_∞ loop-shaping for robust performance and an outer-loop that uses gradient descent with an accurate model of system power consumption to optimize energy efficiency. The convergence of power to its optimal value is exponential and does not require a time-scale separation, which are advantages over published model-free extremum-seeking results e.g., [7], [8]. The result gives a computable robustness margin, scales up to large numbers of zones, and provides a design procedure for each tunable parameter.

The VCS system is described in Section II. Control system requirements are listed in Section III, with an accompanying discussion of a control strategy that meets them. The control laws are derived in Sections IV and V, and simulations and preliminary experimental results are described in Section VI. We draw conclusions and outline future work in Section VII.

II. SYSTEM DESCRIPTION

Consider the VCS operating in heating mode shown schematically in Fig. 1, consisting of one outdoor unit and N indoor units. The outdoor unit contains a receiver, an electronic expansion valve (EEV M), an evaporating heat exchange coil, a compressor and an outdoor fan. The indoor units each contain a condensing heat exchange coil, an EEV and an indoor fan. The $N+3$ controls for the system are the compressor frequency CF, the commanded settings for each EEV i, $1 \leq i \leq N$, EEV M and the outdoor fan speed OFS.

The fan speeds for each indoor unit, IFS i, are set by the customer and are neglected for the remainder of this paper. Each zone is subject to an unknown heat disturbance Q_i.

The system operates by compressing refrigerant to a superheated vapor, which is distributed to each indoor coil via insulated pipes where it releases heat and condenses to a liquid. Subcooled liquid refrigerant exits the indoor coils, is expanded by each EEV i, and returns to the outdoor unit as a two-phase fluid. After the fluid travels through the receiver, it expands again through EEV M and passes as two-phase fluid to the outdoor coil, where it absorbs heat from the outside air and evaporates. It then returns to the compressor as superheated gas. Note that the indoor units are all at a common pressure and condensing temperature, neglecting the pressure drop in the pipes.

An important variable for heat pump control is the subcooling temperature of each indoor coil, T_{SCi}, defined as the difference between the condensing temperature T_C and the measured temperature of the exiting refrigerant, $T_{out\,i}$ for $1 \le i \le N$. There is an *inverse* relationship between T_{SCi} and the heat flux from coil i, as a coil with large values of subcooling will produce refrigerant that is cooler at its exit and a reduced heat flux, in comparison to the heat flux produced by a coil with a small value of subcooling. For a zone with a large negative heat load (relative to the other zones), the refrigerant must be allowed to subcool a *small* amount (relative to the other zones), resulting in a relatively large heat flux from the corresponding indoor coil to meet the load. On the other hand, a zone with a relatively small negative heat load must have a larger amount of subcooling, resulting in a lower heat flux from the indoor coil. This property is used to achieve different zone temperatures and reject asymmetric heat loads.

An important practical consideration is that the measurement of T_C is not always reliable. In normal operation, the refrigerant enters the indoor unit as superheated gas, and cools to the condensing temperature by the time it reaches the upstream sensors located at $T_{in\,i}$, $1 \le i \le N$. In this case, $T_{in\,i}$ is an accurate measurement of T_C and $T_{SCi} = T_{in\,i} - T_{out\,i}$. But in some situations, superheated refrigerant can penetrate into the indoor coil beyond the location of the upstream sensor, making it an inaccurate measurement of T_C. In this case, T_{SCi} is estimated as described in Section IV. One solution would be to move the upstream sensor further downstream. But it is also used in cooling mode, when the refrigerant flow direction is reversed. In cooling mode, the optimal sensor location is at the end of the coil, leading to its compromise location.

III. Control Requirements & Strategy

The controller must satisfy the following requirements:

1) Regulate T_{Ri} to a reference r_i with zero steady-state error for constant values of Q_i and r_i, $1 \le i \le N$.
2) Ensure the refrigerant leaving each indoor unit is subcooled liquid.
3) For the zone with the smallest subcooling, regulate the subcooling, denoted T_{SCmin}, to a reference value r_{sc} with zero steady-state error.
4) Regulate the compressor discharge temperature T_D to a reference value r_d with zero steady-state error, where r_d depends on the outside air temperature T_A and the system load.
5) Achieve a rise time in T_{Ri} for a step input at r_i of τ_R minutes.
6) Minimize the power consumption in steady-state.

The control system must meet these requirements using only the temperature sensors listed in Table II and do so *robustly* for a class of plant model uncertainty described below.

Some remarks are in order. Requirement 1 is met by controlling the amount of subcooling that occurs in each indoor coil, as previously discussed. Requirement 2 ensures energy efficient and quiet operation; if two-phase refrigerant exits the indoor coil, energy efficiency is compromised and undesirable acoustic noise can result as the refrigerant expands across EEV i. Requirement 3 also ensures energy efficient operation by maintaining at least a small amount of positive subcooling, typically a few °C. By regulating the subcooling to a small value, the control system also maintains a proper balance of liquid refrigerant between the indoor units and the outdoor unit; refrigerant imbalances can starve heat exchangers, resulting in lower system efficiency. Requirement 4 maintains the refrigerant cycle at its design conditions throughout the operating envelope, specifically ensuring that the refrigerant at the compressor suction port is superheated (to avoid liquid ingestion) and that the compressor discharge temperature does not exceed design constraints.

The main contribution of this paper is a control system architecture that meets all of these requirements. The ar-

TABLE I
INPUT SIGNALS.

Name	Symbol	Description
T_A	d	Measured outdoor air temperature (°C)
Q_i	q_i	Unmeasured zone i heat load, $1 \le i \le N$ (kW)
OFS	u_0	Outdoor fan speed (kRPM)
CF	u_1	Compressor frequency (Hz)
EEV i	u_{i+1}	Electronic expansion valve i, $1 \le i \le N$ (counts)
EEV M	u_{N+2}	Electronic expansion valve M (counts)

TABLE II
OUTPUT SIGNALS.

Name	Symbol	Description
T_{Ri}	y_i	Zone i Temp., $1 \le i \le N$ (°C)
$T_{in\,i}$	y_{i+N}	Condenser i temp., $1 \le i \le N$, (°C)
$T_{out\,i}$	y_{2i+N}	Condenser i outlet temp., $1 \le i \le N$, (°C)
T_D	y_{3N+1}	Compressor discharge temp. (°C)
T_S	y_{3N+2}	Compressor suction temp. (°C)
T_E	y_{3N+3}	Evaporator temp. (°C)
T_A	y_{3N+4}	Ambient temp. (°C)

TABLE III
ESTIMATED SIGNALS.

Name	Symbol	Description
p_s	z_1	Suction pressure (MPa)
p_d	z_2	Discharge pressure (MPa)

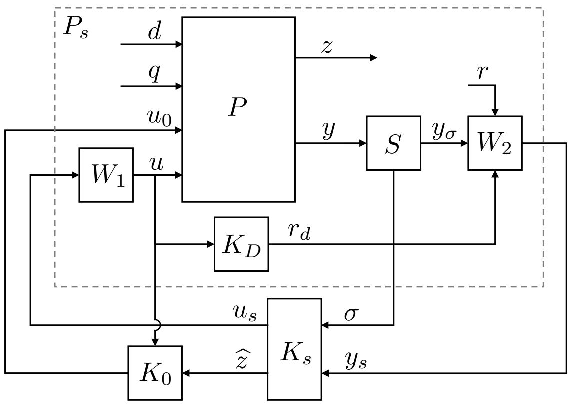

Fig. 2. Block diagram showing the plant P, input and output weights W_1 and W_2, selector function S, compressor discharge temperature schedule K_D, gain-scheduled compensator K_s, and nonlinear power minimizing compensator K_0.

chitecture, shown in Fig. 2, is a cascade of an inner-loop that is designed to regulate key process variables robustly, and an outer-loop designed to drive the power consumption to its minimum. The inner-loop contains compensator K_s, which is designed using H_∞ loop-shaping to regulate the $N+2$ variables T_{Ri}, $1 \leq i \leq N$, T_{SCmin}, and T_D using the $N+2$ controls CF, EEV i, $1 \leq i \leq N$, and EEV M. This design is detailed in Section IV. The outer-loop, containing the nonlinear compensator K_0, actuates the OFS in a manner that minimizes the power consumption for constant values of disturbances and references over the VCS operating envelope. Its design is described in Section V.

IV. Inner-Loop Controller Derivation

Shifting to a control-oriented notation where the signals are described in Tables I - III, the linearized plant model, with nonlinear output, is

$$\begin{aligned} \dot{x} &= Ax + Bu + B_0 u_0 + B_d d + B_q q && (1) \\ y &= Cx && (2) \\ z &= Ex + Fu + F_0 u_0 + F_d d && (3) \\ p &= h(z, u, u_0), && (4) \end{aligned}$$

where x is the state, $u = [u_1, \ldots, u_{N+2}]^T$ is the control input (used in the H_∞ feedback), u_0 is the outdoor fan speed (used in the power minimizing feedback), d is the measured outdoor air temperature, $q \in \Re^N$ is the unmeasured heat load disturbance, y is a vector of measured equipment and zone temperatures, z is a vector of the unmeasured compressor suction and discharge pressures (used to estimate T_C and also in the power minimizing feedback), $p \in \Re_+$ is the system power consumption, and h is a nonlinear model of the power consumption.

The model (1)-(3) is computed by linearizing a detailed system model that is constructed using the *Modelica* modeling language [9], [10], [11]. This model includes a finite volume model of the VCS and a resistor-capacitor type model of occupied spaces that are coupled to the ambient temperature through a wall with standard building constructions. The linearized model is symbolically computed, numerically evaluated at a representative operating condition, and reduced through a sequence of conventional Hankel norm truncations and singular perturbations, giving the low-order model (1)-(3). Equation (4) models the compressor and outdoor fan power consumption as a nonlinear function of OFS, CF, and the suction and discharge pressures, and is described in Section V.

The candidate architecture is shown in Fig. 2. The selector S takes the $3N+4$ measurements y as input and chooses the zone with the minimum subcooling, producing a $2N+4$-dimensional output vector y_σ that is used for feedback. Blocks W_1 and W_2 are weighting functions that are designed by loop-shaping the plant frequency response to meet requirements 1-5, while block K_D is a schedule for the compressor discharge temperature reference. Block K_s is the robustifying compensator computed in the H_∞ loop-shaping synthesis; it has an observer-based structure [12] that is exploited to produce estimates of the unmeasured variables z for the purpose of providing an estimate of T_C. Finally, the block K_0 is the nonlinear gradient descent feedback that drives the system to its minimum system power consumption. Each of these blocks is described in detail below.

A. Selector S

The purpose of the selector is to automatically select the zone with the smallest subcooling for feedback. Define the minimum subcooling as

$$\bar{T}_{SC} = \min_{1 \leq i \leq N} \left(T_C - T_{out\,i} \right), \qquad (5)$$

where T_C is assumed to be measured, and define the selector vector $\bar{\sigma} \in \Re^N$ with elements

$$\bar{\sigma}_i = \tanh\left(\bar{T}_{SC} - (T_C - T_{out\,i}) \right) + 1, \qquad (6)$$

for $1 \leq i \leq N$, which we normalize,

$$\sigma = \bar{\sigma} / \Sigma_{i=1}^{N} \bar{\sigma}_i. \qquad (7)$$

The selector vector σ is a normalized weight that "points" in the direction of the zones with the least amount of subcooling, meaning σ_i is closer to 1 for the least subcooled zones, while those zones with more subcooling will have σ_i closer to zero. It is normalized so that $\Sigma_{i=1}^{N} \sigma_i = 1$, $0 < \sigma_i < 1$, and is C_∞ to provide a smooth transition among gains for the gain scheduled compensator K_s. We remark that a conventional "min select" for selecting the subcooling variable has been observed to cause undesirable chattering type behaviors, and also makes robustness analysis difficult.

The output of the selector is the $2N+4$-dimensional vector

y_σ with elements, for $1 \leq i \leq N$,

$$y_{\sigma i} = y_i = T_{Ri} \quad (8)$$
$$y_{\sigma i+N} = y_{2i+N} = T_{out\,i} \quad (9)$$
$$y_{\sigma 2N+1} = y_{3N+1} = T_S \quad (10)$$
$$y_{\sigma 2N+2} = y_{3N+2} = T_E \quad (11)$$
$$y_{\sigma 2N+3} = y_{3N+3} = T_D \quad (12)$$
$$y_{\sigma 2N+4} = \sum_{i=1}^{N} \sigma_i \left(y_{2i+N} - y_{i+N} \right) =: T_{SCmin} \quad (13)$$

B. Weights $W1$ and $W2$

The $N+2$ variables to be regulated with the $N+2$ controls available in u are $y_{\sigma i} = T_{Ri}$, $1 \leq i \leq N$, $y_{\sigma 2N+3} = T_D$ and $y_{\sigma 2N+4} = T_{SCmin}$. To meet the steady-state tracking and disturbance rejection requirements, we augment "PI" type weights to the six controlled output variables, including integral action. The other measurements $T_{out\imath i}$, $1 \leq i \leq N$, T_S and T_E are weighted so that their gains are less than unity, with no integral action and with some roll-off for robustness. Thus the elements of W_2, labeled for clarity, are

$$T_{Ri}: \quad y_{si} = k_1 \frac{1 + s/\omega_1}{s} (y_{\sigma i} - r_i) \quad (14)$$

$$T_D: \quad y_{s2N+3} = k_2 \frac{1 + s/\omega_2}{s} (y_{\sigma 2N+3} - r_d) \quad (15)$$

$$T_{SCmin}: \quad y_{s2N+4} = k_3 \frac{1 + s/\omega_3}{s} (y_{\sigma 2N+4} - r_{sc}) \quad (16)$$

$$T_{out\,i}, T_S, T_E: \quad y_{sj} = k_4 \frac{1}{1 + s/\omega_4} y_j \quad (17)$$

for $1 \leq i \leq N$ and $N + 1 \leq j \leq 2N + 2$. Note that a positive feedback convention is used, which is common in the H_∞ loop-shaping literature. The gains k_i, $1 \leq i \leq 3$ are tuned so that the shaped plant crossover frequency satisfies the transient response requirement 5. Zeros ω_i, $1 \leq i \leq 3$ are placed to maximize phase margin near crossover, following conventional loop-shaping techniques, and the pole ω_4 is placed so its time constant is about 2-5 minutes. These gains can be designed using the system frequency response and conventional loop-shaping techniques, providing a straightforward model-based design procedure. The input weight $W_1 = I$ for simplicity, but can be used to adjust the contributions of each actuator.

Remark 1: Conventionally W_1 is used to shape the response [12]. But here we use W_2 because we have a non-square disturbance rejection problem with more sensors than actuators. We use all of the available sensors in the feedback to improve the state estimator performance. The disadvantage of this approach is it makes anti-windup design more difficult. Alternatively we can incorporate integral action into W_1, which makes anti-windup easier, but presents some other challenges related to assigning priorities when actuators saturate. These are beyond our scope and will be considered in future work.

C. Compressor Discharge Temperature Schedule K_D

The reference value for T_D (r_d) is scheduled to a value that optimizes system energy efficiency and also ensures positive superheating in the evaporator coil as functions of system load and the outdoor air temperature (d). However, since the load is not measured, we use the compressor frequency CF $= u_1$ as a proxy. We thus define a schedule for the T_D reference as

$$r_d = k_5 \frac{1}{1 + s/w_5} u_1 + k_d d, \quad (18)$$

where the first-order filter is included to improve system robustness, and the gains k_5 and k_d are tuned empirically (these may be nonlinear functions in practice.) This filter is integrated into the plant model, along with the weights W_1 and W_2, to define the shaped plant P_s with input u_s and output y_s; this plant model is shown in Fig. 2.

D. H_∞ Synthesis of K_s

H_∞ loop-shaping controller synthesis [12], [13], [14] computes the controller K_s that minimizes

$$\gamma = \left\| \begin{bmatrix} K_s \\ I \end{bmatrix} (I - P_s K_s)^{-1} \begin{bmatrix} I & P_s \end{bmatrix} \right\|_\infty \quad (19)$$

and robustly stabilizes the family of perturbed plants

$$\tilde{P}_s = \{(M_s + \Delta_M)^{-1}(N_s + \Delta_N) : \ \|\Delta_N \quad \Delta_M\|_\infty < 1/\gamma\}, \quad (20)$$

where Δ_M and Δ_N represent the plant uncertainty and the nominal shaped plant is decomposed into normalized left coprime factors $P_s = M_s^{-1} N_s$. For our purposes, this methodology allows a general formulation of a robust stabilization problem and definition of a multivariable robustness margin ($1/\gamma$) without having to explicitly model the uncertainty, which is difficult for vapor compression system control problems.

The shaped plant is written

$$\dot{x}_s = A_s(\sigma) x_s + B_s u_s + B_{s0} u_0 + B_{sr} r + B_{sd} d + B_{sq} q \quad (21)$$
$$y_s = C_s x_s + D_s r \quad (22)$$
$$z = E_s x_s + F_s u_s + F_0 u_0 + F_d d, \quad (23)$$

where x_s includes the plant, weight and T_D schedule states and A_s, B_s, B_{s0}, B_{sd}, B_{sq}, C_s, E_s, and F_s are the corresponding matrices in (1)-(2) augmented with (14)-(17) and (18) in the usual manner. Note that A_s depends on the selector vector σ, but the other matrices are constant.

The controller K_s has the observer-based structure

$$\dot{\widehat{x}}_s = A_s(\sigma) \widehat{x}_s + B_s u_s + B_{s0} u_0 + B_{sr} r + B_{sd} d + H_s(\sigma)(\widehat{y}_s - y_s) \quad (24)$$
$$\widehat{y}_s = C_s \widehat{x}_s + D_{sr} r \quad (25)$$
$$u_s = G_s(\sigma) \widehat{x}_s, \quad (26)$$

where the control gain G_s and observer gain H_s are both functions of the selector vector σ. Note that the references and measured disturbances are fed forward. The gains G_s

and H_s are computed at particular values of σ by computing solutions to two decoupled Riccati equations [12], [14], and then linearly interpolated. In practice, we find that computing the gains at the N "corner" cases $\sigma = [1\ 0\ \cdots\ 0], \ldots, [0\ \cdots\ 0\ 1]$, giving G_{si} and H_{si} for $1 \leq i \leq N$, and linearly interpolating among them

$$G_s(\sigma) = \Sigma_{i=1}^{N} \sigma_i G_{si}, \quad (27)$$
$$H_s(\sigma) = \Sigma_{i=1}^{N} \sigma_i H_{si}, \quad (28)$$

works well and is easily evaluated for robustness properties at intermediate values of σ.

Because (24)-(26) has an observer-based structure, it may be used to compute estimates of z using (23) that are used in the power-minimizing control K_0. Subtracting (24) from (21) and defining $\tilde{x}_s = x_s - \widehat{x}_s$, the state estimate error is governed by

$$\dot{\tilde{x}}_s = (A_s + H_s C_s)\tilde{x}_s + B_{sq} q, \quad (29)$$

which shows that the observer states will not converge to the plant states for nonzero values of q and will consequently bias estimates of z. However, we can estimate the steady-state value of q (assuming it is constant) by inverting (29), since $\widehat{y}_s - y_s$ is known,

$$\widehat{q} = H_q(\widehat{y}_s - y_s), \quad (30)$$

where

$$H_q = \left(C_s(A_s + H_s C_s)^{-1} B_{sq}\right)^{\dagger}, \quad (31)$$

and the symbol $\dagger$ denotes the pseudoinverse. This inverse exists because q is observable from y_s, and the dimension of y_s exceeds the dimension of q. This estimate can then be used to remove steady-state bias due to q from the estimate of z, giving

$$\widehat{z} = E_s \widehat{x}_s + F_s u_s + F_0 u_0 + F_d d + H_z \widehat{q}, \quad (32)$$

where

$$H_z = -C_s(A_s + H_s C_s)^{-1} B_{sq}. \quad (33)$$

Note that H_q and H_z are functions of σ, and are gain scheduled as in (28).

The estimate of discharge pressure $\widehat{p}_d = \widehat{z}_1$ is used to generate an estimate of the condensing temperature via the refrigerant saturation curve, which is well approximated with a third order polynomial f_s over the operating envelope, i.e.,

$$\widehat{T}_C = f_s(\widehat{p}_d), \quad (34)$$

providing a means to estimate T_C when the upstream temperature sensors in all of the indoor units are not effective. In practice, we use a minimum selector on the measurements and estimates. Closed-loop stability and gain margins are easily validated with $\widehat{T}_C$ feedback, which is used in (5)-(7) and (13). As a fringe benefit, the zone loads q are also estimated, which may be useful for emerging applications. On the other hand, these estimates are sensitive to open-loop plant uncertainty in B_{sq}, which will limit their accuracy.

V. Power Minimizing Feedback

With the inner loop feedback (24)-(26) closed, we consider the SISO system with input u_0 and output p. For constant values of r_i, $1 \leq i \leq N$, d and q, we assume that the steady-state function from u_0 to p is strictly convex for $u_{0min} \leq u_0 \leq u_{0max}$. This property is exploited in model-free extremum-seeking results [15] and is generally satisfied by the VCS. In this work, we use a model-based approach to achieve exponential convergence of power to its minimum value.

The outdoor fan and compressor account for all of the modeled power consumption, so (4) can be written

$$p = h(z, u_0, u_1) = p_c(z_1, z_2, u_1) + p_f(u_0), \quad (35)$$

where the fan power p_f is modeled as a cubic polynomial in fan speed,

$$p_f(u_0) = \gamma_0 + \gamma_1 \cdot u_0 + \gamma_2 \cdot u_0^2 + \gamma_3 \cdot u_0^3. \quad (36)$$

Similarly, the compressor power p_c is modeled as

$$p_c(z_1, z_2, u_1) = \zeta_1(u_1) + \zeta_2(u_1) \cdot z_1 \cdot \eta_V \cdot u_1 \cdot V_{disp} \cdot \left(\frac{z_2}{z_1}\right)^{\zeta_3(u_1)} + \zeta_4(u_1) \cdot z_1 \cdot \eta_V \cdot u_1 \cdot V_{disp}, \quad (37)$$

where the volumetric efficiency is

$$\eta_V(\omega, z_2, z_1) = \theta_1(u_1) + \theta_2(u_1) \cdot \left(\frac{z_2}{z_1}\right) + \theta_3(u_1) \cdot \left(\frac{z_2}{z_1}\right)^2 + \theta_4(\omega) \cdot (z_2 - z_1) + \theta_5(\omega) \cdot z_1 \cdot (z_2 - z_1), \quad (38)$$

V_{disp} is the compressor displacement, $\theta_j(u_1) = \beta_{j0} + \beta_{j1} u_1$, $\zeta_i(u_1) = \alpha_{i0} + \alpha_{i1} u_1 + \alpha_{i2} u_1^2$ for $i = 1, \ldots, 4$ and $j = 1, \ldots, 5$ [16]. The parameters γ_k, α_{ik} and β_{jk} are tuned empirically. Models such as (36)-(38) are used by manufacturers for system design and are known accurately.

Define $\widehat{w} = [\widehat{z}_1\ \widehat{z}_2\ u_0\ u_1]^T$, where we use the estimates of z, so we may write the estimate of (35) compactly as $\widehat{p} = h(\widehat{w})$. Let $T(s)$ denote the 4×1 closed-loop transfer function (with the inner-loop closed) from u_0 to $\widehat{w}$, and define the steady-state gain $T_0 = T(0)$. We then define the power minimizing feedback as the gradient descent,

$$u_0(t) = -\kappa \int_0^t dh\left(\widehat{w}(\tau)\right) \cdot T_0 \, d\tau, \quad (39)$$

with $\kappa > 0$, where the gradient

$$dh = \frac{\partial h}{\partial w}$$

is computed symbolically from (35)-(38). A block diagram is shown in Fig. 3.

Theorem 1: The closed-loop system (1) - (4) with feedback (24)-(26) and (39) is locally exponentially stable for $0 < \kappa < \bar{\kappa}$ for some some (sufficiently small) $\bar{\kappa} > 0$, if

1) references r_i, $1 \leq i \leq N$, and disturbances d and q are sufficiently slowly-varying and
2) $\frac{\partial^2 h}{\partial u_0^2}(T_0 u_0) > 0$.

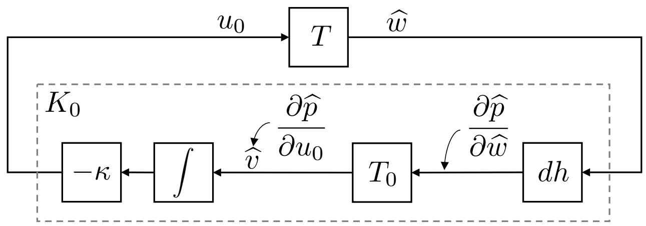

Fig. 3. Power-minimizing feedback loop. The output of the dh block is $\frac{\partial \widehat{p}}{\partial \widehat{w}}$. By the chain rule, the output of the T_0 block is $\frac{\partial \widehat{p}}{\partial u_0}$ at steady-state. The gradient feedback forces $\dot{u}_0 = -\kappa \frac{\partial \widehat{p}}{\partial u_0}$, where $\widehat{p}$ denotes the estimated power, computed using estimates of p_s and p_d. The feedback loop is exponentially stable for sufficiently small $\kappa > 0$.

In this case solutions converge exponentially to the minimum value of power (35) for constant values of r_i, $1 \leq i \leq N$, d and q.

Proof: The inner-loop is exponentially stable by design at fixed σ. Assumption (1) ensures that the gain-scheduled controller is exponentially stable for time-varying σ [17]. We must show that the feedback (39) is locally exponentially stabilizing. Write the SISO system from input u_0 to output $\widehat{v}$ in state space form,

$$\begin{aligned} \dot{\xi} &= A_o \xi + B_o u_0 && (40) \\ \widehat{v} &= dh(C_o \xi) \cdot T_0, && (41) \end{aligned}$$

where (A_o, B_o, C_o) is a realization of T and $\widehat{v}$ is defined in Fig. 3. Without loss of generality, shift the origin of (40)-(41) to the minimum of h (so that $u_0 = 0$ and $\xi = 0$ correspond to the minimum value of p). Assumption (2) implies $dh(-C_o A_o^{-1} B_o u_0) \cdot T_0$, the gradient of $\widehat{p}$ with respect to u_0 in the steady-state, is an odd function that vanishes at $u_0 = 0$, and that dh has a linear term in its Taylor's series at this point. The control (39) is integral type feedback around (40)-(41),

$$u_0 = -\kappa \int_0^t \widehat{v}(\tau)\, d\tau. \qquad (42)$$

The closed-loop is locally exponentially stable for sufficiently small gain κ by a root-locus argument with (41) linearized at the origin, provided the sign of the feedback is negative, which is ensured by T_0. This is because all of the poles of T are in the open left-half plane, and the integral feedback (42) adds a pole at the origin, which will move into the open left-half plane, while the other poles remain in the open left-half plane, for sufficiently small κ. Because ξ converges to 0 exponentially, the power converges to its minimum exponentially. $\square$

In effect (39) drives u_0 to a condition in which dh is orthogonal to T_0, at which point the power is at a local minimum. Note that although the estimated power is used in the feedback, there is no need to invoke any kind of separation principle because the dynamics of the estimate error do not depend on u_0, and the estimator dynamics are explicitly incorporated into T. The gain κ must be limited because T is not non-minimum phase in general, so sufficiently high gain may result in instability. This result is local because dh has higher-order terms that effectively increase the feedback gain for large values of initial conditions, although we do not find this to be a problem in practice. A global result would require a bound on $\|dh\|$ and use of the Circle criteria [18] or similar theory. Finally, we do not find the "slowly-varying" assumption to be practically limiting. In practice the closed-loop system is stable for step changes in references and disturbances, which are expected in any practical realization.

VI. Case Study

We consider a 10kW, four-zone VCS operating in heating mode, described in detail in [4]. A 20^{th}-order model of this system (1)-(3) is constructed as described in Section IV. The weights are tuned to achieve a room temperature rise time of $\tau_R = 15$ min., corresponding to a cross-over frequency of approximately $\omega_C = 0.008\,\mathrm{rad/s}$ for the singular values most aligned with the room temperatures. Tuning the gains is done by inspection of the singular value frequency response, shown in Fig. 4. The TD temperature schedule and reference values for r_{SC} are calibrated empirically. The loop-shaped compensator K_s provides a robustness margin $\gamma = 1.8$, which is excellent for this system and, in our experience, approximately 5x smaller (i.e., more robust) than what is achievable using an LQR/LQG approach with hand-tuning of the weighting matrices[1]. The power minimizing feedback does not adversely affect γ. Conventional model reduction techniques can be applied to reduce the order of K_s by about 3x without seriously compromising performance or robustness.

Fig. 5 shows a closed-loop simulation result where the zone temperature references and the heat loads are changed. The zone temperatures track to their set points with minimal interaction. The selector signal vector σ is also shown, indicating the zone in which subcooling is regulated changes depending on conditions. The lower two plots illustrate the application of the power-minimizing feedback. In the top trace of each plot, the OFS (blue) is set to a constant 940 RPM, i.e., the power-minimizing feedback is turned off, while lower traces (red) show the effect of driving the OFS to its minimum with the power-minimizing feedback turned on. Power is driven to its minimum exponentially with the same time constant as the zone temperature response.

Additionally, the inner-loop H_∞ loop-shaping controller has been implemented on a commercial four-zone heat pump installed in our laboratory, where adiabatic test chambers enclose each of indoor units and the outdoor unit. (A detailed description of the test facility is provided in [4]). The gain-scheduled controller (24)-(26) is discretized with a sample period $T_s = 1$ s. Experimental conditions are chosen such that -1.8 kW (cooling) loads of are applied in each indoor unit chamber, and the outdoor unit chamber temperature is set to 5°C. The VCS is operated in open-loop until steady-state has been reached. Then the observer (24) is engaged

[1] Admittedly, this is an unscientific and incomplete comparison.

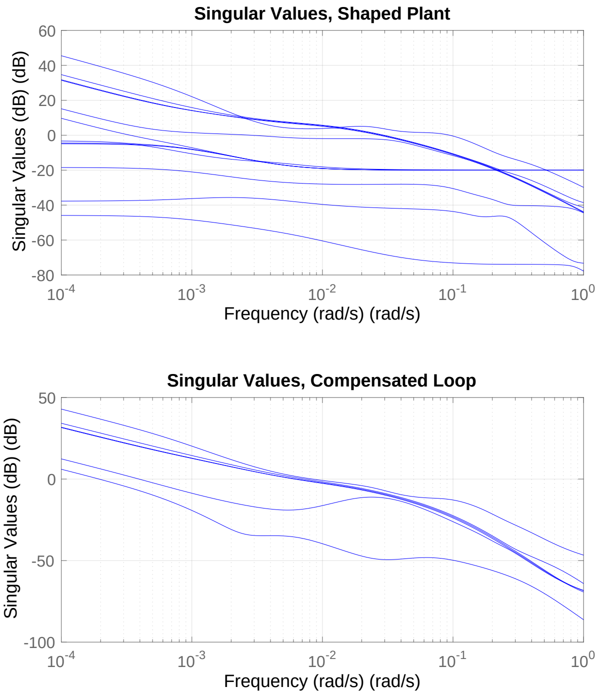

Fig. 4. Shaped plant singular values (top), and compensated loop-shape (bottom). Note the integral action for the 6 regulated variables. The cross-over frequencies for the singular values most associated with room temperatures are approx. $\omega = 0.008\,\mathrm{rad/s}$, corresponding to a rise time of approx. 15 min. Singular values associated with subcooling are slow relative to the others and cannot be made faster for physical reasons.

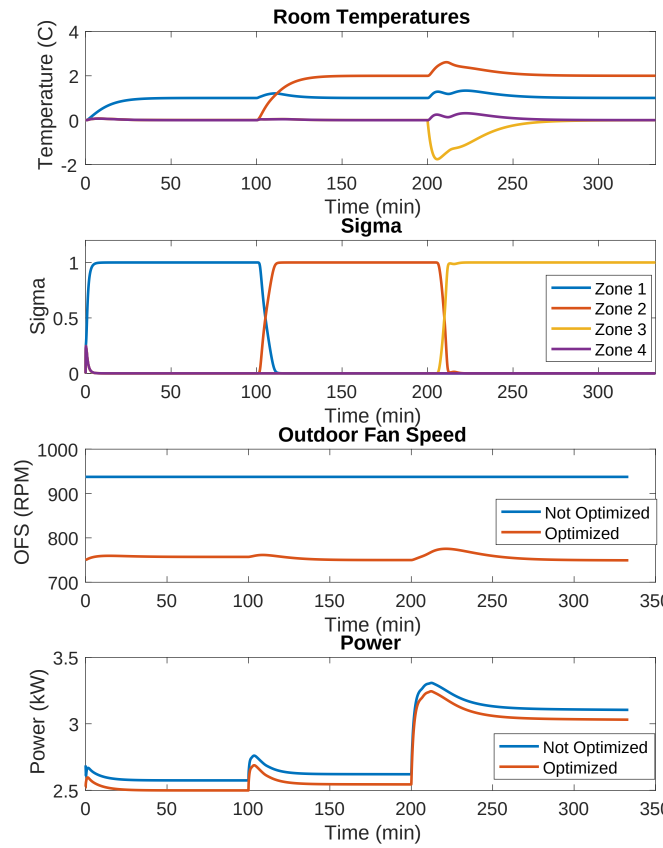

Fig. 5. Zone temperature response (top), selector vector σ (second from top, with legend), OFS (third from top) and power (bottom) due to three transients. At $t = 0\mathrm{min}$ the zone 1 set-point is increased 1°C. At $t = 100\mathrm{min}$ the zone 2 set-point is increased 2°C, which causes the selector to choose zone 2 for subcooling control. At $t = 200\mathrm{min}$ the load in zone 3 is reduced by $1\mathrm{kW}$, resulting in the selector choosing zone 3 for subcooling control. The temperatures in all 4 zones track their set-points with zero steady-state error. The two bottom plots compare a fixed OFS=940RPM (blue) to the OFS regulated by the power optimizing control (red). It is clear that the OFS will track to the value giving the minimum power, exponentially fast.

for 10 min to allow initialization transients to settle, at which time the controller is engaged. Fig. 6 shows the response to two step changes in room temperature set-points. The controller stabilizes the four zones to their respective set-points (top) and the selector (second from top) operates such that the subcooling in zone 4 is regulated to 4°C (third from top), while the discharge temperature is driven to its reference (fourth from top). During the second room temperature set-point change (at $t = 25$ min), a sufficiently high amount of heat is required from zone 1 such that the selector switches from zone 4 to zone 1, and the associated subcooling droops during the transient to provide warmer two-phase refrigerant to raise the temperature in zone 1.

VII. CONCLUSIONS

In this paper, we have presented a new control system architecture for multi-zone air-to-air heat pumps. The architecture is a cascade with an inner-loop designed using H_∞ loop-shaping and an outer-loop designed to drive the system to its minimum power consumption exponentially. The design exploits the observer-based structure of the inner-loop to estimate unmeasured variables and gives an excellent robustness margin, at least for our specific case study.

Some important issues have been left unaddressed in this paper. First, a practical controller must enforce constraints on some states and inputs and incorporate anti-windup. Our single degree-of-freedom design, with the integral weights on the outputs, makes anti-windup difficult to implement. Moving the integral action to the input weight of the single degree-of-freedom design is possible and allows for stable implementation of anti-windup. However, in this design, reference tracking is lost for all signals of interest when a single actuator is saturated. A reference governor may address this problem. This will be described in a future publication.

MPC would explicitly address these problems, and allow for enforcement of state constraints that are neglected in this paper. It would be interesting to consider the inverse optimal control problem of constructing the weighting matrices for MPC from the loop-shaped solution, which would address the robustness issues with MPC.

A second issue is the accuracy of the estimates used in this paper, which depend in part on open-loop models (specifically B_q): these quantities depend on the particular equipment installation and building thermodynamics, and therefore possess uncertainty. Adaptation of some kind may

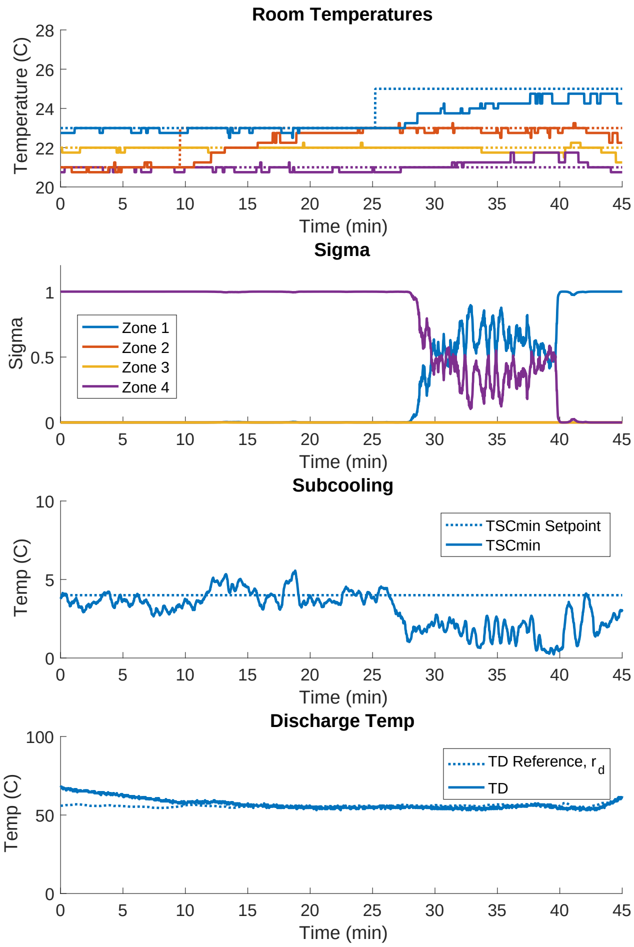

Fig. 6. Experiment demonstrating room temperature regulation of the H_∞ loop-shaping controller. (Top) Room temperatures of four zones. (Second) The selector selects zone 1 after $t = 25$ min to meet the heating requirement. (Third) Subcooling is regulated to 4°C, except when heating demands require reduced subcooling during a transient. (Fourth) Discharge temperature is driven to its reference. Quantization is $0.5°$C on most sensors, causing "noise" in σ, but not adversely affecting closed-loop performance.

enable the process of learning critical system parameters. Finally, it may be possible to design K_s to make the outer loop *passive*, as in [19], in which case the low-gain requirement for the power-minimizing feedback can be removed.

ACKNOWLEDGMENT

We gratefully acknowledge Fumiaki Baba, Takaya Yamamoto, Masashi Fujitsuka, Yuki Mori, and Takahiro Nakai of the Advanced Technology Center, Mitsubishi Electric Corporation, Japan, for their strong collaboration and unwavering support of this work.

REFERENCES

[1] "Buildings and climate change: Summary for decision - makers," UNEP's Sustainable Buildings and Climate Initiative (SBCI), 2009.

[2] Y. T. Wang, D. R. Wilson, and D. F. Neale, "Heat-pump control," *IEEE Proceedings D - Control Theory and Applications*, vol. 130, no. 6, pp. 328–332, November 1983.

[3] X. Zhang, W. Shi, Q. Hu, B. Yan, A. Malkawi, and N. Li, "Distributed temperature control via geothermal heat pump systems in energy efficient buildings," in *2017 American Control Conference (ACC)*, May 2017, pp. 754–760.

[4] D. J. Burns, C. Danielson, S. D. Cairano, C. R. Laughman, and S. A. Bortoff, *Intelligent Building Control Systems: A Survey of Modern Building Control and Sensing Strategies*. Springer, 2017, ch. Model Predictive Control of Multi-Zone Vapor Compression Systems, pp. 105–137.

[5] H. Ferreau, S. Almér, R. Verschueren, M. Diehl, D. Frick, A. Domahidi, J. Jerez, G. Stathopoulos, and C. Jones, "Embedded optimization methods for industrial automatic control," in *Proceedings of the IFAC World Congress*, 2017.

[6] J. Doyle, "Guaranteed margins for lqg regulators," *IEEE Transactions on Automatic Control*, vol. 23, no. 4, pp. 756–757, Aug 1978.

[7] V. Tyagi, H. Sane, and S. Darbha, "An extremum seeking algorithm for determining the set point temperature for condensed water in a cooling tower," in *American Control Conference*, 2006.

[8] P. Li, Y. Li, and J. E. Seem, "Efficient Operation of Air-Side Economizer Using Extremum Seeking Control," *Journal of Dynamic Systems, Measurement, and Control*, vol. 132, no. 3, May 2010.

[9] C. R. Laughman, H. Qiao, D. J. Burns, and S. A. Bortoff, "Dynamic charge management for vapor compression cycles," in *Proceedings of the 23rd International Refrigeration and Air Conditioning Conference*, Purdue University, West Lafayette, IN, 2016.

[10] C. R. Laughman, H. Qiao, S. A. Bortoff, and D. J. Burns, "Simulation and optimization of integrated air-condtioning and ventilation systems," in *Proceedings of the International Building Performance Simulation Assocaition (IBPSA) Conference*, 2017.

[11] H. Qiao, C. R. Laughman, S. A. Bortoff, and D. J. Burns, "Dynamic characteristics of an r410a multi-split variable refrigerant flow air conditioning system," in *Proceedings of the 12th IEA Heat Pump Conference*, 2017.

[12] S. Skogestad and I. Postlethwaite, *Multivariable Feedback Control: Analysis and Design*. Wiley, 2005.

[13] K. Glover and D. McFarlane, "Robust stabilization of normalized coprime factor plant descriptions with h_∞ bounded uncertainty," *IEEE Transactions on Automatic Control*, vol. 34, no. 8, pp. 821–830, 1989.

[14] G. Vinnicombe, *Uncertainty and Feedback: H_∞ Loop-Shaping and the ν-Gap Metric*. Imperial College Press, 2001.

[15] M. Guay and D. J. Burns, "A proportional integral extremum-seeking control approach for discrete-time nonlinear systems," *International Journal of Control*, vol. 90, no. 8, pp. 1543–1554, 2017.

[16] J. Threlkeld, *Thermal Environmental Engineering*. Prentice Hall, 1970.

[17] J. S. Shamma and M. Athens, "Guaranteed properties of gain scheduled control for linear parameter-varying plants," *Automatica*, vol. 27, no. 3, pp. 559–564, 1991.

[18] M. Vidyasagar, *Nonlinear Systems Analysis: Second Edition*. Prentice-Hall, 1993.

[19] T. Hatanaka, X. Zhang, W. Shi, M. Zhu, and N. Li, "An integrated design of optimization and physical dynamics for energy efficient buildings: A passivity approach," in *2017 IEEE Conference on Control Technology and Applications (CCTA)*, 2017, pp. 1050–1057.